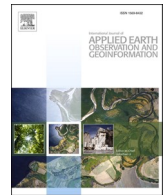




Contents lists available at ScienceDirect

International Journal of Applied Earth Observations and Geoinformation

journal homepage: www.elsevier.com/locate/jag



Mapping individual abandoned houses across cities by integrating VHR remote sensing and street view imagery

Shengyuan Zou, Le Wang*

Department of Geography, University at Buffalo, the State University of New York, Amherst, NY 14261, United States



ARTICLE INFO

Keywords:

Residential housing abandonment
Large-scale mapping
Very-high-resolution remote sensing images
Street view images
Data fusion

ABSTRACT

Abandoned houses (AH) present an utmost challenge confronting the urban environment in contemporary U.S. shrinking cities. Data accessibility is a major hurdle that prevents the acquisition of large-scale AH information at the individual property level. To this end, the latest revolution of open-access remote sensing platforms has witnessed a plethora of multi-source, multi-perspective fine-spatial-resolution data for urban environments, among which very-high-resolution (VHR) top-down view remote sensing images and horizontal-perspective Google Street View (GSV) images are prominent exemplifiers. In this study, we aim to map individual-level abandoned houses across cities by developing a method that can effectively leverage VHR remote sensing and GSV images. The proposed method is composed of four steps. First, we explored the feasibility of the three most relevant and complementary remote sensing data for individual-level AH detection, i.e., daytime VHR images, nighttime light VHR images, and GSV images. Second, we extracted discriminative features that are indicative of housing abandonment conditions from the three disparate data sources. Third, we applied decision-level fusion with Dempster-Shafer Theory (DST) to better leverage the prior knowledge about data effectiveness. In the last step, a geographical random forests (GRF) model was first implemented to improve the predictions of where houses were occluded on GSV images. We mapped individual AH in two typical U.S. shrinking cities, Buffalo, NY, and Cleveland, OH, which allowed us to further explore the individual-property-level spatial characteristics of AH. Results revealed that the proposed DST fusion and GRF prediction consistently achieved promising performance across the two cities. Given the merits of incorporating open-access and multi-perspective data, our proposed method has the potential to be generalized to understanding regional and national-scale urban environments tackling housing abandonment challenges.

1. Introduction

Abandoned houses (AH) refer to residential properties whose owners chose to give up their ownership, thus leading to long-term vacancy and significant vandalism (Mallach, 2018; U.S. General Accounting Office, 1978). As its dramatically increasing number achieved 5.6 million in 2011, housing abandonment (HA) became a prominent problem across the U.S. (Accordino and Johnson, 2000; U.S. Government Accountability Office, 2011). Consequently, abandoned houses brought devastating social impacts on the local societies associated with population loss and deterioration of the urban environment, including declining housing markets, rising crime rates, and local government's financial burden (Molloy, 2016; Raleigh and Galster, 2015; Silverman et al., 2013). It should be noted that HA is a pervasive problem across different regions in the U.S. (Accordino and Johnson, 2000; Mallach,

2018; U.S. Government Accountability Office, 2011). Therefore, it is imperative to derive extensive HA information for better housing and built environment management, particularly along with the ongoing revitalization of many U.S. shrinking cities (Lynch and Mosbah, 2017).

Conventionally, three primary datasets, i.e., American Housing Survey (AHS) (Dewar and Thomas, 2012; Mallach, 2018), United States Postal Service (USPS) administrative data (Silverman et al., 2013), and nighttime light (NTL) imagery (Pan and Dong, 2020; Wang et al., 2019) have been employed to derive large-scale HA information. However, these data sources can only work at an aggregated level, and thus cannot meet the needs of urban studies at the finest scale. Regarding that, individual-property-level abandonment information is essentially needed to extend our understanding of urban shrinkage and related urban studies, e.g., small-area population and built environment estimation (Chen et al., 2021; Suel et al., 2021). It can also assist decision-

* Corresponding author.

E-mail addresses: szou2@buffalo.edu (S. Zou), lewang@buffalo.edu (L. Wang).

Table 1

Existing data sources for AH detection, which can be categorized into two groups: survey data and image data.

Category	Data sources	Limitation	Reference
Category 1	Field survey data	Labor-consuming data collection	Hillier et al., 2003; Yin and Silverman, 2015; Konomi et al., 2019
Category 2	Utility data Very-high-resolution remote sensing images	Accessibility Effectiveness	Kumagai et al., 2016; Deng and Ma, 2015; Zou and Wang, 2020
	Google street view images	Occlusion	Zou and Wang 2021

making by local government and real estate managers in urban planning and housing markets. To this end, a handful number of studies, which can be grouped into two categories depending upon their employed data sources (Table 1), have been reported for detecting individual-level abandoned houses.

The first category employed field data, including data collected through field surveys, tele-surveys, self-reporting systems, and utility companies (Hillier et al., 2003; Konomi et al., 2019; Kumagai et al., 2016; Yin and Silverman, 2015) (Category 1 in Table 1). Although field data is the prevalent data source that can achieve high accuracy, it has several major limitations, i.e., costly collection, poor accessibility, and inconsistent quality. Such limitations seriously constrained previous studies to a small geographical extent, e.g., a city (Zou and Wang, 2021). The second category employed remotely sensed image data that can address these limitations, including very-high-resolution (VHR) remote sensing images and street view images (Deng and Ma, 2015; Zou and Wang, 2020, 2021) (Category 2 in Table 1). VHR remote sensing imagery can infer housing vacancy and abandonment by presenting

abnormal surrounding vegetation conditions (Zou and Wang, 2020). Towards a similar direction, street view images, e.g., Google Street View (GSV) images, can be utilized to distinguish AH from others by presenting deteriorated building facades and overgrown front yards (Zou and Wang, 2021). Both VHR and GSV images have public accessibility, large-extent coverage (covering almost all U.S. cities), and fine spatial resolution (Anguelov et al., 2010; Toth and Józkow, 2016), thus emerging as two potential candidates to scale up to address HA problem across different cities.

The weaknesses of image data sources, however, are notable as well. The efficacy of VHR remote sensing is limited because it provides information no more than building rooftops and surrounding vegetation conditions, which can only be utilized as secondary indicators. Also, its efficacy has not been proven for large-scale mapping. Alternatively, the street view imagery cannot cover every residential house due to occlusion caused by trees and other objects, making it difficult to map every AH in a given region. Therefore, no matter top-down view or street view, a single remotely sensed data source cannot suffice as a cost-effective method to detect individual AH at a large scale.

A possible solution to overcome the abovementioned limitations is integrating multi-sourced remotely acquired data in individual AH mapping. The marriage of top-down view and street view imagery will combine their advantages and overcome their weaknesses. Particularly, street view images, which are captured by cameras on vehicles, can provide rich horizontally observed information about the urban environment (Biljecki and Ito, 2021); on the other hand, top-down view imagery can observe information (including houses and yards) that are horizontally occluded. The integration of top-down view and street view images can merge the visual clues from two different viewing perspectives and improve performance in many urban remote sensing topics (Cao et al., 2018; Law et al., 2019; Suel et al., 2021).

Specifically, building-related urban studies that integrated VHR remote sensing and street view images has emerged recently and mainly

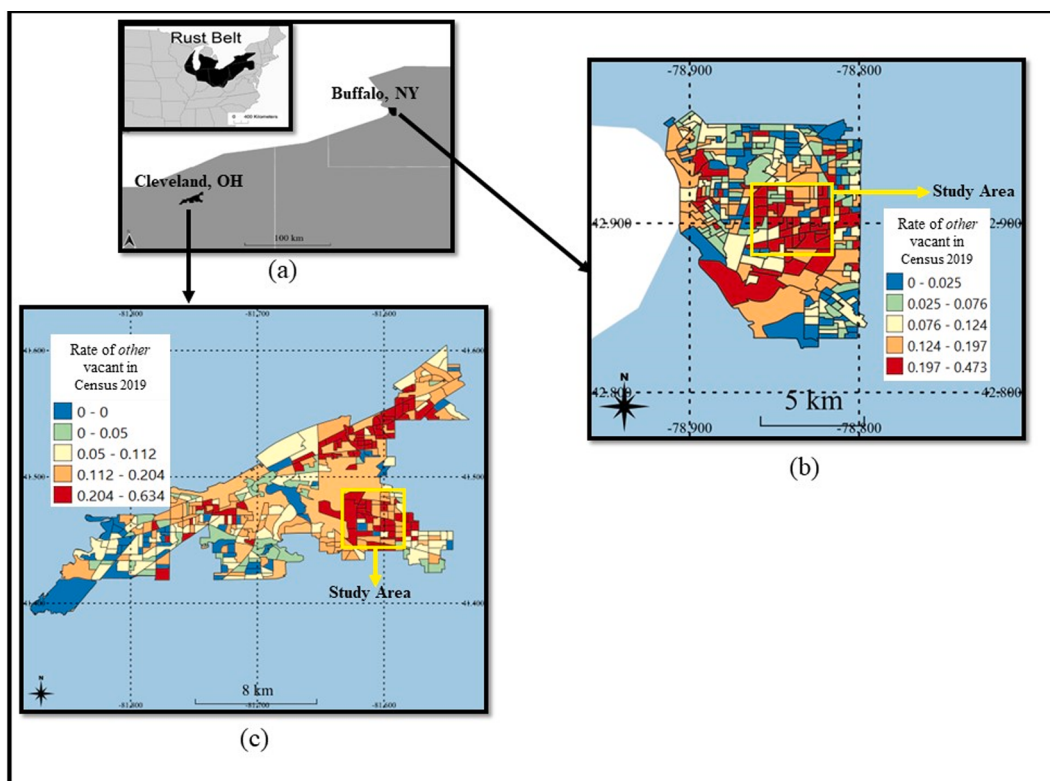


Fig. 1. Two study areas, corresponding to two yellow squares in the figure, are hyper-vacancy regions in Buffalo, NY, and Cleveland, OH. (a) Locations of Buffalo and Cleveland in the Rust Belt region. (b) Distribution of the rate of 'other' vacant properties (the closest definition to AH in Census ACS data) in Buffalo in 2019. (c) Distribution of the rate of 'other' vacant properties in Cleveland in 2019.

Table 2
List of datasets used in this study.

Data sources	Buffalo, NY	Cleveland, OH	Purpose
VHR daytime imagery	NYS GIS Clearinghouse in 2017	USDA NAIP data in 2017	Data source to derive AH data
Street view imagery	GSV	GSV	Data source to derive AH data
VHR NTL imagery	JL1-3B in Sep. 2017	Unavailable	Data source to derive AH data
Reference data	In Rem Auction data in 2018 and 2019	Parcel Tax Bill Summary in 2018 and 2019	Reference
Parcel data	Available in 2019	Available in 2019	Assisting segmentation and providing housing market condition variables
Census ACS data	Available in 2017	Available in 2017	Providing socioeconomic variables

focused on three topics: building/land use classification (Cao et al., 2018), house price estimation (Law et al., 2019), and building information modeling (Yu et al., 2019). The building/land use classification method proposed by Cao et al. (2018) is the first building-information-related work that integrated remote sensing and street view images and demonstrated the effectiveness. In their proposed method, features extracted from remote sensing images and street view images were fused in a deep convolutional neural networks (DCNN) model. Besides building/land use classification, house price estimation is another cutting-edge application integrating VHR remote sensing and street view. As the pioneering one, the work proposed by Law et al. (2019) extracted feature vectors from images then integrated them in traditional hedonic models. Furthermore, to model detailed building information, e.g., exterior construction material, story (floor), year of built, a DCNN-based framework was proposed by Yu et al. (2019) to extract visual features of buildings from VHR and street view images. The effectiveness of the proposed framework was demonstrated through experiments on a large-scale image database. Therefore, integrating top-view VHR and street view in building-related urban studies serves an effective and efficient avenue for large-scale urban management, thus making it a cutting-edge interdisciplinary area.

However, as spatially sparse street view images result in blank in spatially continuous mapping, integration at locations where occlusion happens is unimplementable. Therefore, improving mapping results where occlusion happens is meaningful yet undeveloped. To conclude, while integrating multi-perspective image data is expected to be a cost-effective method, efforts are needed to investigate how to implement integration in AH mapping and improve performance.

The solution to the above problem will directly facilitate addressing a profound geographic question: what is the spatial characteristic of individual AH between different cities? As a key indicator of urban shrinkage and environment decay, the spatial distribution of housing vacancy and abandonment needs investigation (Baba and Asami, 2017). Previous studies only explored the spatial distribution at coarse spatial resolution or in a small geographical extent due to data limitations (Morckel, 2014b&2015; Yin and Silverman, 2015). Accordingly, findings and conclusions drawn in previous studies may differ at different spatial scales across different study areas. To this end, fine-resolution investigation across cities will extend our understanding of the spatial distribution of AH associated with the different urban environments.

The objective of this study is to explore the feasibility of mapping individual-level abandoned houses across cities by integrating multi-perspective remotely sensed datasets and further explore the spatial characteristics of AH at the individual level. In particular, 1) we aim to develop a new AH mapping method integrating VHR remote sensing images and GSV images and to establish an optimal model for large-scale

individual-level mapping; 2) we aim to implement the developed method in two U.S. shrinking cities, Buffalo, NY, and Cleveland, OH, to investigate the individual-property-level spatial distribution of AH.

2. Study area and data

There are two study areas (Fig. 1): one is in the city of Buffalo in upstate New York, U.S., and the other is in the city of Cleveland, OH, U.S. Both cities are located in the Rust Belt region (Fig. 1a), where is a major concentration of AH and has suffered an industry and population decline since the 1970 s. An acute level of HA substantially impacts the neighborhoods in both cities. We selected one representative subset study area from each city (the yellow squares in Fig. 1b&c), both of which are in hyper-vacancy residential neighborhoods with significant interests in exploring the HA problem.

There are six datasets utilized in this study (Table 2). Three image data sources were utilized to map abandoned houses: 1) VHR remote sensing image datasets: New York State Digital Orthoimagery data in 2017 for Buffalo, NY, from New York State (NYS) Geographical Information Science (GIS) Clearinghouse (<https://gis.ny.gov/gateway/mg/2017/erie/>), and Digital Ortho Photo Imagery data from National Agriculture Imagery Program (NAIP) in 2019 for Cleveland, OH (https://datagateway.nrcs.usda.gov/GDGHome_DirectDownload.aspx). Both open-access and free-download VHR image datasets have four spectral bands (visible and near-infrared) and submeter-level spatial resolution (0.3 m for NYS GIS orthoimages in Buffalo and 0.6 m for NAIP orthoimages in Cleveland); 2) VHR nighttime light image: one scene of Jilin1-3B (JL1-3B) image captured on September 25th, 2017 for Buffalo, which is the first new-generation high-resolution NTL satellite imagery with submeter spatial resolution (0.98 m) and three visible bands (Zheng et al., 2018); 3) Street view imagery: Google Street View imagery, which is the largest street view dataset with the broadest coverage including all cities in the U.S. Raw GSV images were collected by retrieving and downloading images through Google Street View Static API. In image retrieving and downloading, the input of retrieval is parcel addresses, and the photograph facing the input address taken at the nearest image-taking location will be returned automatically, which indicates that the viewpoint and focal length were adapted to the target parcel address. The horizontal maximum field of view was set as 120 degrees. The vertical angle of the camera was 0 degrees. The output size of the image was 640 × 640 pixels. Based on residential parcel addresses, 9,523 GSV images in Buffalo and 16,683 images in Cleveland were collected. Indoor images, repetitive images, and images without buildings were filtered out in preprocessing. At last, 5,934 GSV images in Buffalo and 7,071 GSV images in Cleveland were reserved for AH prediction.

Datasets for references and assistance include: 1) In Buffalo, In Rem Auction Results Archive (open access: <https://data.buffalony.gov/>) in 2018 and 2019 was utilized as reference data. The In Rem auction is run by the Department of Assessment and Taxation with the goal of recovering unpaid property taxes and utility bills by selling the property at auction. To be specific, 107 residential properties that were in *adjourned* and *struck* categories in two years, both of which categories indicated unsold abandoned houses, were counted as ground-truth samples. To collect a comparable number of occupied houses (OH), other 200 residential property samples through visual interpretation from GSV images as OH ground-truth data. This dataset, including 307 properties, was utilized to estimate data sources in Section 3.3 and act as a basic training dataset combined with local training set, which includes 500 GSV-based visual interpretation samples for each site for further classification. Thus, we have 807 training samples in total for each study site. In Cleveland, open-access Parcel Tax Bill Summary data (<https://clevelandgis.maps.arcgis.com/apps/webappviewer/index.html?id=f15dec13ee6648bc218d4f5c8290691>) was employed as validation data. This dataset was collected based on the occupancy status of the parcel owner and late tax payment penalty in their parcel

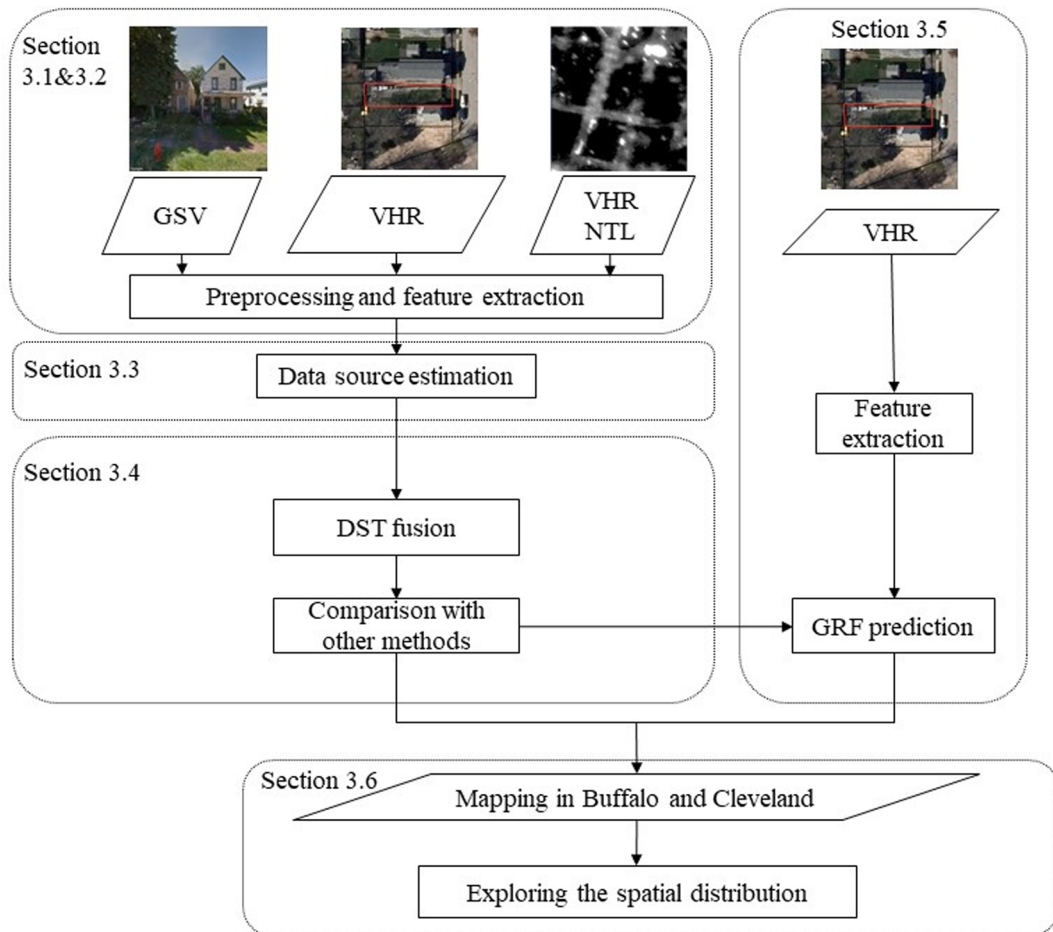


Fig. 2. Workflow of this study. Multi-source image datasets are integrated in AH mapping.

tax bill summary and manually cross-validated in their historical GSV images. If a residential parcel's occupancy status of its owner is *Not* and it has a late tax payment penalty and significant deterioration on its historical street view image, this parcel was treated as an abandoned parcel with AH. This data, as the best reference data we knew, acted as validation data in Cleveland to evaluate the generalization of the proposed method. 2) Buffalo parcel data in 2017 from NYS GIS Clearinghouse (<https://gis.ny.gov/gisdata/inventories/details.cfm?DSID=1300>) and Cleveland parcel data in 2019 from Cuyahoga County Open Data (<https://datacuyahoga.opendata.arcgis.com/datasets/combined-parcels-cleveland-only/>) were utilized to segment remote sensing images into parcels for object-based feature extraction and classification. The reason to choose parcel boundary in remote sensing image segmentation is that tax parcel, as the smallest unit in urban property studies, has fewer irrelevant objects than fixed-size grids (Suel et al., 2021) and other road-derived vectors (Zhong et al., 2020), thus can present building condition more accurately for this individual-property-level study. Parcel datasets also provide housing market variables for spatial characteristic investigation in this study. There are 10,014 residential parcels in our study area in Buffalo and 16,683 in Cleveland. 3) US Census American Community Survey (ACS) data at the census block group level in the year of 2017 provides socioeconomic variables.

3. Method

In practice, there are two scenarios when detecting abandoned houses through integrating remote sensing and street view imagery: 1) For residential properties that have available GSV imagery, the prediction could be implemented by integrating information from top-view

and street-view remote sensing; 2) For residential properties without available GSV, the prediction will only rely on remote sensing imagery thus cannot benefitting from the integration. To this end, we proposed a further step to improve the prediction results in the second scenario by employing the prediction results in the first scenario and implementing a geographical random forests (GRF) model (Georganos et al., 2021). The proposed method is supposed to be more predictive when using the better predictions (Scenario 1) to improve others (Scenario 2), at the same time addressing the observed spatial heterogeneity of HA.

The whole approach of this study is presented in Fig. 2, which can be divided into six steps: 1. Image datasets were preprocessed, including filtering out unsuitable GSV images and segmenting VHR remote sensing images; 2. Visual features, e.g., building façade, front yard vegetation, surrounding vegetation, and NTL intensity, were extracted from corresponding image datasets; 3. The image datasets, including VHR daytime imagery, VHR NTL imagery, and street view imagery, were estimated in a random forests (RF) classifier based on the classification accuracy and the out-of-bag (OOB) errors of their features; 4. We implemented the theory of evidence to fuse decisions from separate decision trees based on different data sources. The proposed integration method was compared with other ensemble methods based on validation results in Buffalo and Cleveland; 5. As the optimal integration results can be determined, these results will act as training samples when building up local GRF models to predict abandonment status of houses that were occluded on GSV images; 6. Individual-level AH maps were generated in two study sites, covering over 25,000 residential properties. We explored the spatial characteristics of AH to understand this phenomenon in two cities. Details are presented from Sections 3.1 to 3.6.

Table 3

Sixteen visual features extracted from image datasets for AH detection.

Data source	Feature index	Features (16 in total)	References
VHR NTL (4 features)	1 2 3 4	Mean intensity, Total intensity, Lit area, Lit area ratio	Du et al., 2018; Pan and Dong, 2020
Daytime VHR (9 features)	5 6 7 8 9 10 11 12 13	Mean band R, Mean band NIR, Standard deviation band R, Standard deviation band NIR, GLCM entropy band R, GLCM entropy band NIR,	Deng and Ma, 2015; Zou and Wang, 2020
GSV (3 features)	14 15 16	Mean NDVI, GLCM homogeneity band R, GLCM homogeneity band NIR, Scene-based score, Building patch ratio, Vegetation patch ratio	Zou and Wang 2021

3.1. Preprocessing

This section presents preprocessing of VHR remote sensing images, GSV images, and reference data in sequence. Since pixels are grouped into objects in VHR images, the whole image processing approach of VHR images is based on objects, which refer to tax parcels. The preprocessing is required to filter out non-building parcels and extract object-based features that can infer HA. Specifically, both VHR daytime images and VHR NTL images were segmented into parcels based on tax parcel boundaries. Residential parcels were chosen as our research targets based on their land-use code in parcel data. To filter out residential parcels without building, we used a Morphological Building Index (MBI) (Huang and Zhang, 2011) to detect whether a building exists within a parcel on the VHR image. As an indicator of building presence, MBI was extracted, refined, and aggregated from pixel to parcel (Zou and Wang, 2020). Only high-MBI parcels (9,523 in Buffalo and 16,683 in Cleveland) were reserved for further mapping. In addition, the grayscale brightness of VHR NTL images was calculated based on Equation (1) (Zheng et al., 2018) to present light intensity in each pixel.

$$\text{Brightness} = 0.2989 \times \text{Red} + 0.5870 \times \text{Green} + 0.1140 \times \text{Blue} \quad (1)$$

Resulting from its uncontrolled quality, raw GSV images that have occlusion and misregistration problems are unsuitable for AH detection. We utilized a ready-made scene recognition DCNN model (Kang et al., 2018), i.e., VGG16 model (Simonyan and Zisserman, 2014) trained on the Places365 dataset (Zhou et al., 2016), to identify if building exists in the central part (320×320) of the image. Images without identified buildings are filtered out. As a result, we obtained 5,934 from 9,523 GSV images in Buffalo and 7,071 from 16,683 in Cleveland that can be used to detect AH.

To ensure the integration of images is geographically correct, we implemented image-to-image registration for geometric correction between VHR daytime and NTL images. We manually checked the geographical position between VHR images and parcel data, both of which did not need additional correction. As the top-view images were segmented based on address-specific parcel boundaries and GSV images were also retrieved and collected based on parcel addresses, features extracted from the image segments and GSV images can match based on their parcel addresses.

3.2. Feature extraction

Features were extracted separately from remote sensing data and GSV data in this section. First, parcel-based features were extracted from remote sensing images. We selected four spectral features (Feature 1–4 in Table 3) from NTL VHR images and nine spectral and texture features from daytime VHR images (Feature 5–13 in Table 3) based on previous studies. In detail, mean intensity, total intensity, lit area, and light area ratio in NTL images were utilized in previous coarse-resolution housing vacancy studies (Du et al., 2018; Pan and Dong, 2020) and proven effective in inferring housing vacancy. Alternatively, for features from daytime remote sensing images, previous studies strongly suggested that abandonment status was related to the surrounding vegetation conditions in terms of overgrown vegetation and eroded/destroyed concrete surface, e.g., mean Normalized Difference Vegetation Index (NDVI) and spectral and texture features, e.g., Gray-Level Co-Occurrence Matrix (GLCM) entropy, in red (R) and near-infrared (NIR) bands (Deng and Ma, 2015; Zou and Wang, 2020). This study followed these conclusions and included the above-examined VHR features in the classification.

In terms of GSV features, we utilized a recently developed hierarchical model based on DCNN to extract features from GSV images at the scene level and the patch level (Zou and Wang, 2021). The traditional scene-based DCNN model can extract scene-level features to identify the probability of AH within the scene of a certain image, so-called scene-based score. Also, detailed patch-level features can be extracted by identifying deteriorated building façade patches and out-of-maintenance front-yard lawn patches. Specifically, patches were square-shaped connected regions of the image automatically extracted based on multi-scale pyramid histogram of visual words (Bosch et al., 2007) features. Next, these patches were divided into building patches and vegetation patches by a ready-made VGG16 model. Then, we developed two new VGG16 models to identify deteriorated building patches and out-of-maintenance vegetation patches. The shares of patches in bad condition within an image are calculated for each category and named as building patch ratio and vegetation patch ratio. Therefore, three multi-scale features were extracted through this hierarchical model (Feature 14–16 in Table 3).

3.3. Data source estimation

To estimate the effectiveness of data sources, we evaluated out-of-bag (OOB) errors of features from different data sources in RF classification and compared the prediction accuracy of five RF models using different combinations of data sources. RF is a fast and accurate classifier to deal with hyper-dimensional data and is able to overcome overfitting with a small number of samples (Breiman, 2001).

Z-score normalization was performed for remote sensing features in each study area before classification to overcome the spectral disturbance due to different sensors and environments. Five RF classification models were trained corresponding to five combinations of features from different data sources: 1) using features from all three image datasets, 2) using features from two VHR remote sensing datasets, 3) using features from VHR daytime remote sensing images and GSV images, 4) using features from VHR daytime images only, and 5) using features from GSV images only. OOB errors and the accuracy of these models will guide us in determining the effective datasets in AH mapping.

3.4. Feature integration

Features extracted from multiple sources need to be integrated in decision-making. In this section, we implemented a decision-level fusion method based on Dempster-Shafer theory (DST) (Shafer, 1992) and compared its performance with other ensemble methods in AH mapping. Training samples for each study site contain the basic training set and the local sample set to simulate the situation in large-scale mapping that

Table 4

Calculation of mass, support, and plausibility probability in DST fusion of GSV and VHR data sources.

<i>A</i>	m_{GSV}	m_{VHR}	m	$\text{Sup}(A)$	$\text{Sup}(\bar{A})$
<i>AH</i>	$w_1 p_1$	$w_2 p_2$	$\frac{1}{K} w_1 p_1$	$m(AH)$	$1 - m(AH)$
<i>OH</i>	$w_1(1-p_1)$	$w_2(1-p_2)$	$\frac{1}{K} w_1(1-p_1) w_2(1-p_2)$	$m(OH)$	$1 - m(OH)$
$AH \cup OH$	0	0	0	1	0

needs a global training database and local training samples to adjust the model for new study areas.

3.4.1. Decision fusion based on Dempster-Shafer theory

We developed a decision fusion framework to fuse decisions from image data sources based on regression trees (RT) and the Dempster-Shafer theory of evidence (Shafer, 1992). DST fusion, which has been applied to GIS studies with some success (Maplica, et al., 2007; Silvan-Cardenas et al., 2010), allows assigning belief weights to each source to leverage external knowledge, i.e., the prior knowledge about data effectiveness in this study.

Two RT were trained based on street view features and remote sensing features, correspondingly, whose output was the predicted probabilities of belonging to AH from each data source. The DST allows us to combine all evidence from different sources (VHR and GSV) to calculate the probability of an event, i.e., whether the house is abandoned or not, by using degree of belief and plausible reasoning. Let S denote a set of basic events. The DST assigns a belief mass to each element of the power set 2^S as a function $m: 2^X \rightarrow [0,1]$ if it satisfied two conditions: $m(\emptyset) = 0$, and $\sum_{A \in 2^S} m(A) = 1$. For each event in the power set, the DST provides representations of both imprecision and uncertainty through the definition of two measures called support (Sup) and plausibility (Pls). These measures are defined in Equations (2) & (3) as follows:

$$\text{Sup}(A) = \sum_{B \in A} m(B) \quad (2)$$

$$\text{Pls}(A) = \sum_{B \cap C \neq \emptyset} m(B) \quad (3)$$

The rule to combine evidence is defined as a joint mass assignment m for two independent mass assignments, m_1 and m_2 in Equations (4) & (5):

$$m(A) = \frac{\sum_{B \cap C = A} m_1(B)m_2(C)}{1 - K} \quad (4)$$

$$K = \sum_{B \cap C \neq \emptyset} m_1(B)m_2(C) \quad (5)$$

In this study, the DST fusion method combined two sources of evidence: (1) from the RT based on street view features; (2) from the RT based on VHR features. There are three non-null events: AH, OH, and $AH \cup OH$. For each house, the probability mass, support, and plausibility of each event are calculated as shown in Table 4, where p_1 and p_2 are the belief parameters, and w_1 and w_2 are the weights. The belief that the house in the GSV image (p_1) or in the VHR remote sensing image (p_2) is abandoned was determined based on the probability from RT, and the weight of each data source (w_1 and w_2) was set to 2/3 and 1/3 based on a preliminary test. Finally, a house was determined as AH if the support for AH was greater than the support to OH.

3.4.2. Comparison with other methods

Besides DST fusion method, we also applied Naïve Bayes (NB) classification, RF classification, and two two-stage approaches. One of them employed RT for each data source in the first stage and fused the multi-source predictions in a NB classification in the second stage. The other

one used NB classification for the first stage and decision trees for the second stage. Validation results from models were compared in terms of accuracy and consistency. Five hundred addresses were randomly selected as validation samples in each city and manually checked their abandoned status through reference data (GSV in Buffalo, Tax Bill Summary data in Cleveland).

3.5. GRF prediction

For the scenario that houses are occluded on GSV images, the prediction only using VHR data will have low accuracy due to the lack of street-view information. To deal with this problem, we developed a solution to improve the prediction by implementing GRF and employing the previous results from integration. The idea of GRF is to consider their locations in the computation by disaggregating the global model to local ones. We propose to employ predictions from locations with GSV data as training samples to predict locations without available GSV data. To be specific, for each training location, the nearest 500 training samples in Euclidean distance, whose HA status has been predicted from integration, were utilized to build the local RF model only using VHR features. For each location without available GSV image, abandonment status is predicted by the nearest local RF model.

There are two contributions when implementing GRF in this study: 1. Local prediction without GSV data can be improved by involving more accurate and nearby training samples, as the occlusion problem can be alleviated by using integration results. 2. Spatial heterogeneity is considered when using local models.

3.6. Investigating the individual-property-level spatial distribution

Based on the developed methods, individual-level AHs were first automatically mapped in two study areas in Buffalo and Cleveland. We generated individual AH maps and aggregated the property-level HA to the block group level. A spatial lag logistic regression model was developed to explore the relationship between HA and its contributing factors. Two categories of factors were involved as independent variables in this study: 1) housing market condition factors, including market value and living area in square feet, which were existing attributes in parcel data, and 2) socioeconomic factors, including the median of age (residents), poverty rate, unemployment rate, and non-white rate, which were collected from Census ACS 5-Year Estimates at the census block group level and assigned to each parcel acting as neighborhood effect. All factors were considered as factors contributing to people's decisions in the housing market in related studies (Bassett et al., 2006; Immergluck, 2016; Mallach, 2018). In detail, poverty rate was calculated by dividing the population below poverty level by the total population. Unemployment rate is calculated by dividing unemployed population (including below, at, or above poverty level) by the population in labor force. And non-white rate is the proportion of non-white population in the census block. Since the spatial autocorrelation of HA and its factors are significant (Mikelbank, 2008; Morckel, 2014b), a spatial lag logistic regression model was established to account for spatial autocorrelation in evaluating the relationship between the above factors and individual-level HA. The spatial lag model in Equation (6) includes a spatially lagged dependent variable (Wy) to average the neighboring values of a location, thus accounting for spatial autocorrelation in the model, where the probability of HA (p) is dependent on its neighbors (Anselin and Rey, 2014). Neighbors are defined by spatial weights. In this study, spatial weights (W) are generated based on inverse Euclidean distance with a 250 m bandwidth. X is the matrix of independent variables, ρ and β are parameters, and ε is a vector of error terms.

$$\ln(p/1-p) = (\rho)Wy + X(\beta) + \varepsilon \quad (6)$$

Table 5

Prediction accuracy using different combinations of datasets in preliminary data source estimation.

Data sources	GSV+ Daytime VHR + NTL VHR	GSV + Daytime VHR	Daytime VHR + NTL VHR	Daytime VHR	GSV
OA	82.4%	81.8%	78.2%	78.5%	76.2%
Precision	75.2	73.4%	70.8%	71.6%	69.3%
Recall	73.8%	74.8%	63.6%	63.6%	57.0%
Kappa	0.61	0.60	0.51	0.51	0.45
F-1 score	0.75	0.74	0.67	0.67	0.63

4. Results

4.1. Data source estimation

Five RF models were tested regarding five combinations of data sources, and their prediction accuracy was listed in [Table 5](#). The Overall Accuracy (OA) using all features extracted from VHR daytime, VHR NTL, and GSV data is 82.4%, and the kappa coefficient is 0.61, which indicates substantial agreement with reference data ([Table 5](#)). This is the

highest prediction accuracy among all combinations, while the model using GSV and daytime VHR data has similar accuracy. Notably, both precision (user's accuracy) and recall (producer's accuracy) of AH are 10% lower than of OH in the detection. In this model, OOB errors were estimated as the importance of features. As shown in [Fig. 3](#), features from the VHR NTL image were not as important as features from the other two data sources in the classification. Next, the model's accuracy using two remote sensing datasets (daytime VHR and VHR NTL images) was assessed. The OA, 78.2%, is lower than the model using all features ([Table 5](#)), and the major drawback is precision. In other words, detection using models without GSV features missed a significant number of AH. Alternatively, the OA of the model only using daytime VHR images is 78.5%, and the kappa coefficient is 0.51, presenting the effectiveness of daytime VHR data. Furthermore, the classification accuracy using GSV was 76.2% ([Table 5](#)). Same with only using remote sensing images, the recall when only using GSV images is relatively lower than integrating both, indicating considerable omission errors. Based on these results, integrating remote sensing and GSV images performs better than using any single data source by significantly ameliorating the occurrence of omission error. In addition, the prediction accuracies that exclude VHR NTL data are almost the same as those that include VHR NTL data ([Table 5](#)), which indicates that the involvement of VHR NTL features

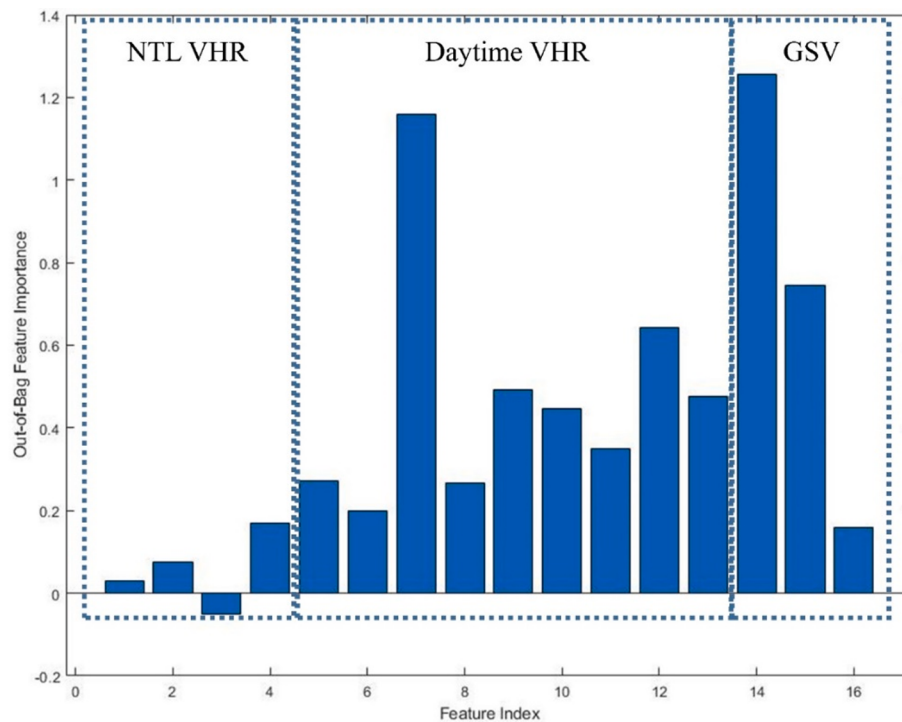


Fig. 3. Data source importance evaluation results based on feature OOB errors in random forests AH classification. Features from NTL VHR images have the lowest importance.

Table 6

Validation results using DST fusion and other ensemble methods to integrate VHR and GSV images in AH detection.

Study site	Data	Method	OA	Kappa	F-1 score	Precision	Recall
Buffalo	VHR + GSV	NB	82.4%	0.29	0.39	36.1%	42.0%
		RF	88.5%	0.42	0.48	61.4%	31.9%
		RT + NB	74.8%	0.22	0.36	27.3%	52.2%
		NB + DT	84.6%	0.35	0.44	43.1%	44.9%
		DST	90.0%	0.58	0.66	61.0%	72.5%
Cleveland	VHR + GSV	NB	81.6%	0.30	0.41	40.5%	41.0%
		RF	71.0%	0.24	0.38	69.2%	26.5%
		RT + NB	75.6%	0.22	0.36	30.4%	45.5%
		NB + DT	81.8%	0.37	0.47	42.7%	53.5%
		DST	78.0%	0.50	0.67	64.7%	68.8%

Table 7

Validation results using VHR images and GRF prediction in Buffalo and Cleveland.

Study site	Data	Method	OA	Kappa	F-1 score	Precision	Recall
Buffalo	VHR	RF	70.4%	0.15	0.24	16.2%	44.2%
		GRF	89.4%	0.33	0.39	48.6%	32.7%
Cleveland	VHR	RF	84.8%	0.13	0.21	22.7%	19.2%
		GRF	85.4%	0.26	0.34	32.2%	36.5%

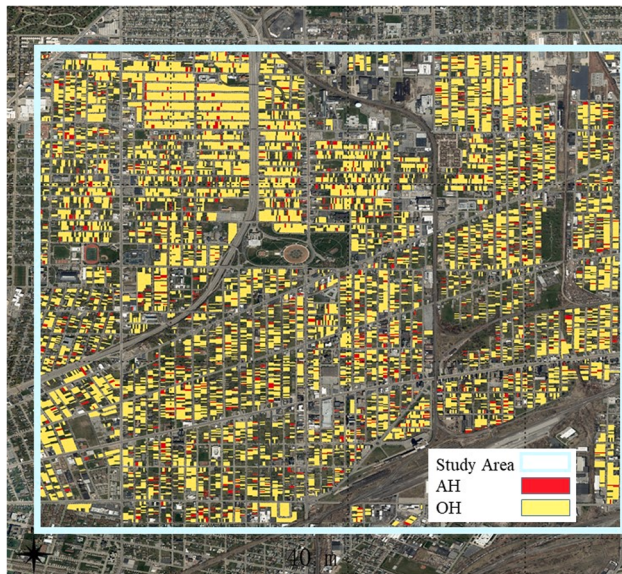


Fig. 4. Abandoned house map in the study area in Buffalo integrating top-view and street view images using DST and GRF method. 1,034 red parcels are predicted individual-level abandoned houses. 8,489 yellow parcels are occupied houses.

does not affect the classification accuracy. Therefore, we decided not to include this ineffective but costly commercial dataset in further approach.

4.2. Classification validation

In fusion model validation, as shown in Table 6, DST fusion has better prediction accuracy than others in terms of kappa coefficient and F-1 score in both cities. DST fusion has the highest recall and the second highest precision among all models, indicating its ability to detect AH more accurately and comprehensively. The kappa coefficient decreases significantly in Cleveland when generalizing the RF model trained in Buffalo. Compared with RF, DST fusion is more consistent.

Generally, predictions only using VHR images have notably lower kappa coefficient and F-1 score than using VHR and GSV. As shown in Table 7, the proposed GRF method significantly improved the results from the RF method in both kappa and F-1 score in both Buffalo and Cleveland. Contributions come from precision in Buffalo and both precision and recall in Cleveland. Therefore, GRF was employed in AH mapping for cases without available GSV.

4.3. Spatial characteristics of AH in two study sites

We mapped AH in two study sites in Buffalo and Cleveland using DST and GRF for the two scenarios (whether GSV data is available or not). Specifically, in Buffalo, we mapped 9,523 residential parcels in total, 5,934 of which were predicted by the model using daytime VHR and GSV features and the DST fusion method, and the other 3,589 predicted by the GRF model using daytime VHR features. 1,034 AH were detected in Buffalo (Fig. 4), where the percentage of AH was 10.9%. In Cleveland,

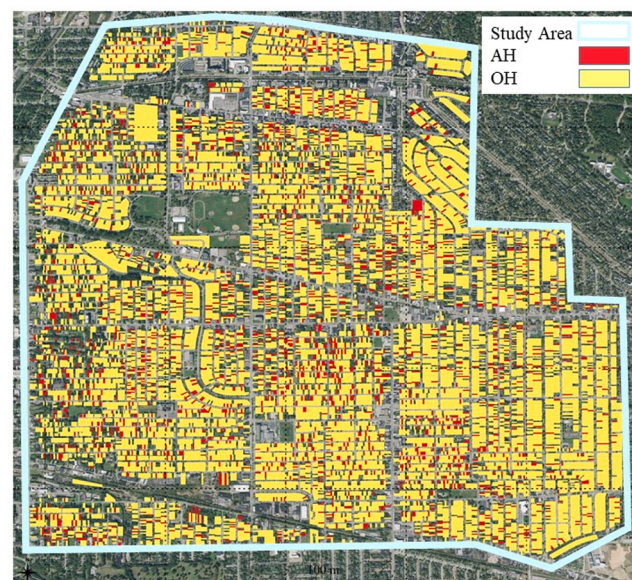


Fig. 5. Abandoned house map in the study area in Cleveland integrating top-view and street view images using DST and GRF method. 2,542 red parcels are predicted individual-level abandoned houses. 14,141 yellow parcels are occupied houses.

we mapped 16,683 residential parcels, 7,671 of which were predicted by integrating GSV and daytime VHR data, and the other 9,012 were predicted by GRF model. As shown in Figs. 5, 2,542 AH were detected in this study site, counting 15.2% of total predictions.

The spatial distribution within the study areas was presented distinctly when aggregating individual-level results to block group level (Fig. 6a&b). In the study area in Buffalo, the southwest districts have a higher percentage of AH, while the north side is a low-abandonment part (<10%). Abandoned houses are more concentrated on the east side rather than the west side in this region (Fig. 6a). In the study area in Cleveland, AH more concentrated on the west side (Fig. 6b). These findings are consistent with the distribution of other vacant properties (as shown in Fig. 1), which is the most relative Census ACS data.

More importantly, this is the first time that abandoned house information is derived at the individual housing level from image datasets, thus making it possible to explore the spatial characteristics at the finest spatial resolution across cities. We found two notable characteristics of AH at the individual property level: 1. AH tend to appear adjacent to another AH (red circle in Fig. 7); 2. AH tend to appear adjacent to vacant lands (dashed red circle in Fig. 7). As both cities demolished thousands of AH during the last several years, these small vacant lands in residential neighborhoods were likely to be AH before the demolition.

As shown in Table 8, housing market value is the only consistently significant factor in the HA problem, which is statistically significant ($p < 0.001$) in both Buffalo and Cleveland. The negative coefficients indicate that when a house has a lower market value, no matter where it is, it has a higher probability of being abandoned. Another statistically significant variable in Cleveland is the living area. Smaller houses in Cleveland indicate a higher probability of being abandoned. Among

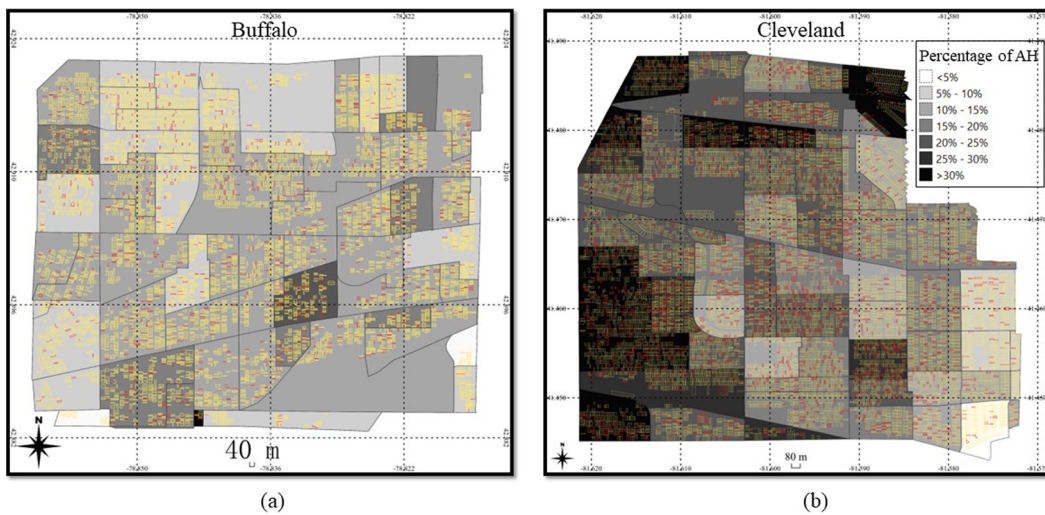


Fig. 6. Distribution of AH (individuals & block groups) in study areas in (a) Buffalo and (b) Cleveland. Darker color indicates higher percentage of abandoned houses in the census block group.

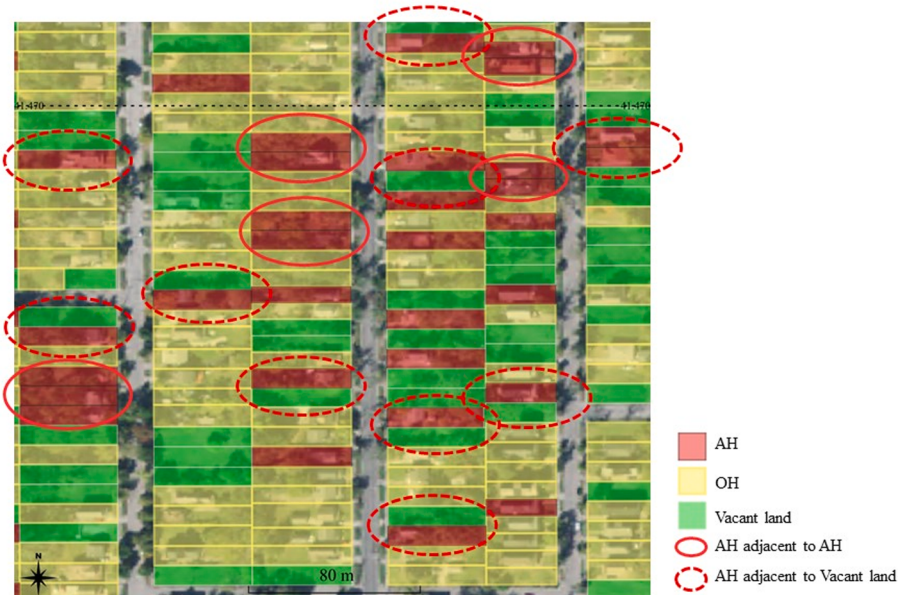


Fig. 7. A typical area where AH (red parcels) tend to be adjacent to each other and vacant lands (green parcels). Pairs are highlighted by solid and dashed red circles, correspondingly.

Table 8
Regression coefficients of the spatial lag HA model in Buffalo and Cleveland.

Contributing factors	Buffalo, NY		Cleveland, OH	
	Coefficient	Significance p	Coefficient	Significance p
Market value	-1.39e-5	<0.001***	-1.70e-5	<0.001***
Living area (sqft)	6.06e-6	0.92	-1.27e-4	0.02*
Median of age	6.09e-4	0.87	7.66e-4	0.80
Poverty rate	7.05e-1	0.08	-5.68e-1	0.002**
Unemployment rate	7.67e-2	0.87	1.61e-1	0.39
Non-white rate	-1.01e-1	0.71	5.49e-1	0.26

* $p < 0.05$,

** $p < 0.01$,

*** $p < 0.001$.

socio-economic factors, the poverty rate in Cleveland is the only significant contributing factor to HA. However, it is counterintuitive that a higher poverty rate implies a lower possibility of abandonment. Besides, all other socioeconomic factors have insignificant effects at the individual property level.

5. Discussion

This study developed the first individual AH mapping method that only relies on open-access image data sources. We examined three data sources and five ensemble methods to intelligently utilize information from multi-perspective images. Furthermore, we implemented a GRF model to improve the occluded predictions on street view images. The individual-level spatial characteristics of AH were first explored across two cities. Detailed contributions, findings, and limitations were discussed as follows.

5.1. Contributions and findings

Our proposed method of integrating two mainstream open-access data has demonstrated great potential for mapping AH at large geo-spatial scales. The employed low-cost and open-access image data sources with a wide spectrum of geographical coverage are inevitably needed merits for large-scale AH mapping. Along this line, we further validated the generalizability of our method as evidenced by the similar prediction accuracy in two different cities (Table 6&7). In addition, we resonated with previous studies that the visual pattern of AH on images is a more consistent indicator of HA across different cities than socio-economic variables (Morckel, 2014a).

We found that the proposed DST and GRF methods, corresponding to two scenarios, are effective in improving predictions in AH mapping. As mentioned above, data gathered from disparate viewing perspectives provide explicit yet complementing clues regarding HA. The improvement in effectiveness in Table 5 results from the refined recall accuracy, which means more abandoned houses can be distinguished due to the features collectively observed from different perspectives. The outstanding result from DST fusion is reasonable since it intelligently utilized the fact that predictions from GSV is more accurate than from VHR and needs higher weights in final decision. In addition, the proposed GRF method successfully leveraged the better predictions from integration to ameliorate accuracy loss due to spatial heterogeneity and occlusion when only using VHR data. The proposed GRF method is the first method against the occlusion problem from a geographical perspective, which has great potential to apply in other urban topics that integrate street view images and other data sources to improve predictability. Going forward, we envision that the proposed multi-perspective data integration and self-improvement scheme will facilitate remote sensing to be applied to address many unresolved urban environmental challenges.

Our method opened a new avenue to investigate the spatial patterns of individual-property-level AH. Comparing with previous studies (Mikelbank, 2008; Wilson et al., 1994; Yin and Silverman, 2015), this is the first investigation of individual-property-level spatial characteristics of AH across different cities with a consistent data quality. AH presents the trend to be adjacent, regarding that current and demolished AH (vacant lands) tend to appear continuously in space. Previous studies have claimed a similar finding at multiple scales in Columbus, Ohio (Morckel, 2014a, 2015) but first demonstrated at the individual property level across cities, implying a spatial propagation trend of this phenomenon may happen universally.

5.2. Uncertainty and limitations

There are three factors to be considered when generalizing the proposed method: the complexity of housing appearance, the various imaging conditions of GSV imagery, and the limited generalizability of remote sensing features. First, the proposed model lacks the capacity to account for the new variance of housing appearance not encountered in the model calibration stage when generalizing to another place. Second, the imaging conditions, e.g., the distance between the camera and the target house, affected the quality of building façade appearing on the GSV image. Third, the generalizability of remote sensing features is limited, which was caused by the difference in vegetation conditions, vegetation maintenance policies, roofing and pavement materials, and VHR sensors in different regions. To tackle these challenges, further study may involve more local training samples for new study sites to calibrate the model and improve the prediction accuracy, which has been proven in a preliminary test. For further large-scale applications, place-based feature extraction methods may also be developed. Other classification and data fusion methods, e.g., the multimodal deep learning approach (Suel et al., 2021), and other open-access data sources, e.g., social media data, are worth exploring in further study.

Another notable uncertainty source is time inconsistency between

GSV and remote sensing datasets. As GSV images were captured at much different dates, the time of taking GSV images cannot match the capture time of remote sensing images. Within the time gap, the appearance and abandonment status of a building may change over time, thus leading to prediction errors. In addition, both omission and commission errors may exist in our GSV-based interpretation ground-truth data. As a potential solution, historical GSV images, which are available only for viewing in some regions through Google Maps, may help to ameliorate the effect from the time gaps.

6. Conclusions

This paper proposed the first individual-level AH mapping method that integrates two open-access image datasets. The integration of top-view and street view imagery was demonstrated effective in AH mapping, which can be further extended to a regional and national-scale AH mapping. Particularly, the proposed GRF model is the first solution to ameliorate the impact from occlusion in GSV, thus having great potential in further integration applications. The adjacent negative impact from existed AH was first demonstrated at the individual property level. Besides providing a new avenue to understanding the spatial characteristics, the detection results have potential in fine-resolution population and built environment estimation for urban management.

CRediT authorship contribution statement

Shengyuan Zou: Conceptualization, Data curation, Methodology, Writing – original draft. **Le Wang:** Conceptualization, Investigation, Supervision, Writing – review & editing.

Declaration of Competing Interest

The authors declare that they have no known competing financial interests or personal relationships that could have appeared to influence the work reported in this paper.

References

- Accordino, J., Johnson, G.T., 2000. Addressing the vacant and abandoned property problem. *Journal of Urban Affairs* 22 (3), 301–315.
- Anguelov, D., Dulong, C., Filip, D., Frueh, C., Lafon, S., Lyon, R., Ogale, A., Vincent, L., Weaver, J., 2010. Google street view: Capturing the world at street level. *Computer* 43 (6), 32–38.
- Anselin, L., Rey, S.J., 2014. Modern spatial econometrics in practice: A guide to GeoDa. *GeoDa Press LLC, GeoDaSpace and PySAL*.
- Baba, H., Asami, Y., 2017. Regional differences in the socio-economic and built-environment factors of vacant house ratio as a key indicator for spatial urban shrinkage. *Urban and Regional Planning Review* 4, 251–267.
- Bassett, E.M., Schweitzer, J., and Panken, S., 2006. Understanding housing abandonment and owner decision-making in Flint, Michigan: An exploratory analysis. *Lincoln Institute of Land Policy Working Paper*, pp.1–62.
- Biljecki, F., Ito, K., 2021. Street view imagery in urban analytics and GIS: A review. *Landscape and Urban Planning* 215, 104217.
- Bosch, A., Zisserman, A., Munoz, X., 2007. In: October. Image classification using random forests and ferns. *Ieee*, pp. 1–8.
- Breiman, L., 2001. Random forests. *Machine learning* 45 (1), 5–32.
- Cao, R., Zhu, J., Tu, W., Li, Q., Cao, J., Liu, B., Zhang, Q., Qiu, G., 2018. Integrating aerial and street view images for urban land use classification. *Remote Sensing* 10 (10), 1553.
- Chen, H., Wu, B., Yu, B., Chen, Z., Wu, Q., Lian, T., Wang, C., Li, Q., Wu, J., 2021. A New Method for Building-Level Population Estimation by Integrating LiDAR, Nighttime Light, and POI Data. *Journal of Remote Sensing* 2021, 1–17.
- Deng, C., Ma, J., 2015. Viewing urban decay from the sky: A multi-scale analysis of residential vacancy in a shrinking US city. *Landscape and Urban Planning* 141, 88–99.
- Dewar, M. and Thomas, J.M. eds., 2012. *The city after abandonment*. University of Pennsylvania Press.
- Du, M., Wang, L., Zou, S., Shi, C., 2018. Modeling the census tract level housing vacancy rate with the Jilin1-03 satellite and other geospatial data. *Remote Sensing* 10 (12), 1920.
- Georganos, S., Grippa, T., Niang Gadiaga, A., Linard, C., Lennert, M., Vanhuyse, S., Mboga, N., Wolff, E., Kalogirou, S., 2021. Geographical random forests: a spatial extension of the random forest algorithm to address spatial heterogeneity in remote sensing and population modelling. *Geocarto International* 36 (2), 121–136.

- Hillier, A.E., Culhane, D.P., Smith, T.E., Tomlin, C.D., 2003. Predicting housing abandonment with the Philadelphia neighborhood information system. *Journal of Urban Affairs* 25 (1), 91–106.
- Huang, X., Zhang, L., 2011. Morphological building/shadow index for building extraction from high-resolution imagery over urban areas. *IEEE Journal of Selected Topics in Applied Earth Observations and Remote Sensing* 5 (1), 161–172.
- Immergluck, D., 2016. Examining changes in long-term neighborhood housing vacancy during the 2011 to 2014 US national recovery. *Journal of Urban Affairs* 38 (5), 607–622.
- Kang, J., Körner, M., Wang, Y., Taubenböck, H., Zhu, X.X., 2018. Building instance classification using street view images. *ISPRS journal of photogrammetry and remote sensing* 145, 44–59.
- Konomi, S.I., Sasao, T., Hosio, S., Sezaki, K., 2019. Using ambient WiFi signals to find occupied and vacant houses in local communities. *Journal of Ambient Intelligence and Humanized Computing* 10 (2), 779–789.
- Kumagai, K., Matsuda, Y., Ono, Y., 2016. Estimation of housing vacancy distributions: Basic Bayesian approach using utility data. *The International Archives of Photogrammetry, Remote Sensing and Spatial Information Sciences* 41, 709.
- Law, S., Paige, B., Russell, C., 2019. Take a look around: using street view and satellite images to estimate house prices. *ACM Transactions on Intelligent Systems and Technology (TIST)* 10 (5), 1–19.
- Lynch, A.J., Mosbah, S.M., 2017. Improving local measures of sustainability: A study of built-environment indicators in the United States. *Cities* 60, 301–313.
- Mallach, A., 2018. The empty house next door. Lincoln Institute of Land Policy, Cambridge, MA.
- Mikelbank, B.A., 2008. Spatial analysis of the impact of vacant, abandoned and foreclosed properties. *Federal Reserve Bank of Cleveland*.
- Molloy, R., 2016. Long-term vacant housing in the United States. *Regional Science and Urban Economics* 59, 118–129.
- Morckel, V.C., 2014a. Spatial characteristics of housing abandonment. *Applied Geography* 48, 8–16.
- Morckel, V., 2014b. Predicting abandoned housing: does the operational definition of abandonment matter? *Community Development* 45 (2), 122–134.
- Morckel, V.C., 2015. Does the house or neighborhood matter more? Predicting abandoned housing using multilevel models. *Cityscape* 17 (1), 61–70.
- Pan, J., Dong, L., 2020. Spatial Identification of Housing Vacancy in China. *Chinese Geographical Science* 1–17.
- Raleigh, E., Galster, G., 2015. Neighborhood disinvestment, abandonment, and crime dynamics. *Journal of Urban Affairs* 37 (4), 367–396.
- Shafer, G., 1992. Dempster-shafer theory. *Encyclopedia of artificial intelligence* 1, 330–331.
- Silvan-Cardenas, J.L., Wang, L., Rogerson, P., Wu, C., Feng, T., Kamphaus, B.D., 2010. Assessing fine-spatial-resolution remote sensing for small-area population estimation. *International Journal of Remote Sensing* 31 (21), 5605–5634.
- Silverman, R.M., Yin, L., Patterson, K.L., 2013. Dawn of the dead city: An exploratory analysis of vacant addresses in Buffalo, NY 2008–2010. *Journal of Urban Affairs* 35 (2), 131–152.
- Simonyan, K. and Zisserman, A., 2014. Very deep convolutional networks for large-scale image recognition. *arXiv preprint arXiv:1409.1556*.
- Suel, E., Bhatt, S., Brauer, M., Flaxman, S., Ezzati, M., 2021. Multimodal deep learning from satellite and street-level imagery for measuring income, overcrowding, and environmental deprivation in urban areas. *Remote Sensing of Environment* 257, 112339.
- Toth, C., Józków, G., 2016. Remote sensing platforms and sensors: A survey. *ISPRS Journal of Photogrammetry and Remote Sensing* 115, 22–36.
- U.S. General Accounting Office, 1978. Housing abandonment: A national problem needing new approaches.
- U.S. Government Accountability Office, 2011. Vacant properties: Growing number increases communities' costs and challenges.
- Wang, L., Fan, H., Wang, Y., 2019. An estimation of housing vacancy rate using NPP-VIIRS night-time light data and OpenStreetMap data. *International Journal of Remote Sensing* 40 (22), 8566–8588.
- Wilson, D., Margulis, H., Ketchum, J., 1994. Spatial aspects of housing abandonment in the 1990s: The Cleveland experience. *Housing Studies* 9 (4), 493–510.
- Yin, L., Silverman, R.M., 2015. Housing abandonment and demolition: Exploring the use of micro-level and multi-year models. *ISPRS International Journal of Geo-Information* 4 (3), 1184–1200.
- Yu, Q., Wang, C., Cetiner, B., Yu, S.X., McKenna, F., Taciroglu, E. and Law, K.H., 2019. Building information modeling and classification by visual learning at a city scale. *arXiv preprint arXiv:1910.06391*.
- Zheng, Q., Weng, Q., Huang, L., Wang, K., Deng, J., Jiang, R., Ye, Z., Gan, M., 2018. A new source of multi-spectral high spatial resolution night-time light imagery—JL1-3B. *Remote sensing of environment* 215, 300–312.
- Zhong, Y., Su, Y., Wu, S., Zheng, Z., Zhao, J., Ma, A., Zhu, Q., Ye, R., Li, X., Pellikka, P., Zhang, L., 2020. Open-source data-driven urban land-use mapping integrating point-line-polygon semantic objects: A case study of Chinese cities. *Remote Sensing of Environment* 247, 111838.
- Zou, S., Wang, L., 2020. Individual vacant house detection in very-high-resolution remote sensing images. *Annals of the American Association of Geographers* 110 (2), 449–461.
- Zou, S., Wang, L., 2021. Detecting individual abandoned houses from google street view: A hierarchical deep learning approach. *ISPRS Journal of Photogrammetry and Remote Sensing* 175, 298–310.